Journal of Power Sources 247 (2014) 605–611

Contents lists available at ScienceDirect

Journal of Power Sources

journal homepage: www.elsevier.com/locate/jpowsour

Short communication

Combinatorial discovery of Ni-based binary and ternary catalysts for hydrazine electrooxidation for use in anion exchange membrane fuel cells

Tomokazu Sakamoto [a, *], Koichiro Asazawa [a], Jean Sanabria-Chinchilla [b, 1], Ulises Martinez [c], Barr Halevi [c, 2], Plamen Atanassov [c], Peter Strasser [d], Hirohisa Tanaka [a]

[a] Frontier Technology R & D Division, Daihatsu Motor Co., Ltd., 3000 Yamanoue, Ryuo, Gamo, Shiga 520–2593, Japan
[b] Department of Chemical and Biomolecular Engineering, University of Houston, Houston, TX 77204, USA
[c] Chemical & Nuclear Engineering Department, UNM Center for Emerging Energy Technologies, University of New Mexico, Albuquerque, NM 87131, USA
[d] The Electrochemical Energy, Catalysis, and Materials Science Laboratory, Department of Chemistry, Chemical Engineering Division, Technical University Berlin, 10623 Berlin, Germany

HIGHLIGHTS

- The electrocatalysts for hydrazine oxidation were investigated by combinatorial chemistry.
- The binary $Ni_{0.8}Zn_{0.2}$ and $Ni_{0.9}La_{0.1}$ showed high activity for hydrazine electrooxidation.
- The best $Ni_{0.8}Zn_{0.1}La_{0.1}$ was optimized by rapid parallel screening.
- XRD analysis indicated that alloying effect improves the catalytic activity.
- Maximum power density was exhibited 486 mW cm^{-2} by $Ni_{0.87}Zn_{0.13}$ as an anode catalyst.

ARTICLE INFO

Article history:
Received 2 June 2013
Received in revised form
20 July 2013
Accepted 27 August 2013
Available online 12 September 2013

Keywords:
Direct hydrazine hydrate fuel cells
Anion exchange membrane fuel cells
Combinatorial chemistry
Hydrazine oxidation
Ni-based binary and ternary catalysts

ABSTRACT

Ni-based catalysts, binary Ni–M (with M = Mn, Fe, Zn, La) and ternary Ni–Mn–Fe and Ni–Zn–La were investigated for hydrazine oxidation in direct hydrazine hydrate fuel cell anodes by a temperature controlled 16-channel electrochemical combinatorial array. The binary $Ni_{0.8}Zn_{0.2}$ and $Ni_{0.9}La_{0.1}$ catalysts are significantly more active than the Ni reference catalyst for hydrazine oxidation. While the best $Ni_{0.8}Zn_{0.1}La_{0.1}$ ternary catalyst is close to the high active binary catalysts in composition. Additionally, $Ni_{0.6}Fe_{0.2}Mn_{0.2}$ catalysts also showed high catalytic activity for hydrazine oxidation in alkaline media over standard Ni catalyst. The X-ray diffraction (XRD) analysis indicated that the alloying effect between Ni and added elements improves the catalytic activity for hydrazine oxidation. As a result of the screening tests and our previous research, unsupported binary $Ni_{0.87}Zn_{0.13}$ and $Ni_{0.9}La_{0.1}$ catalysts were synthesized by spray pyrolysis and tested in a direct hydrazine hydrate fuel cell MEA (DHFC) producing 486 mW cm^{-2} and 459 mW cm^{-2}, respectively.

1. Introduction

Direct liquid fuel cells, such as the methanol, ethanol, borohydride, formic acid and hydrazine hydrate systems, are attractive candidates for electronics applications, because of their high energy density. Especially, direct methanol fuel cells (DMFCs) have been under intensive research within the last 20 years for portable electronics applications such as mobile phones, mp3 players and notebooks. However, to become commercially viable DMFCs have to overcome cost and availability barriers caused by the reliance on Pt and Pt-based catalysts in both anode and cathode electrodes. Moreover, methanol permeation from anode to cathode through membranes, significantly decreasing the FC performance and durability. Direct hydrazine hydrate fuel cells (DHFCs) have been also studied since the 1960s [1–3]. In Japan, the Governmental

* Corresponding author. Tel.: +81 748 1685; fax: +81 748 57 1064.
E-mail address: tomokazu_sakamoto@dk.daihatsu.co.jp (T. Sakamoto).
[1] Present address: Centro de Electroquímica y Energía Química (CELEQ), Universidad de Costa Rica, San José, Costa Rica.
[2] Present address: Pajarito Powder, 317 Comercial St NE, Suite 300, Albuquerque, NM 87102, USA.

0378-7753/$ – see front matter © 2013 Elsevier B.V. All rights reserved.
http://dx.doi.org/10.1016/j.jpowsour.2013.08.107

Industrial Research Institute, Osaka (GIRIO), Panasonic and Daihatsu Motor Co. Ltd. produced an alkaline type hydrazine-air fuel cell vehicle experimentally in 1972, and driving tests were carried out [4]. Recent developments in DHFCs technology have led to full-sized demonstration indicating their feasibility and promise in future fuel cell vehicles [5–8]. Therefore hydrazine electrooxidation electrodes and reaction mechanism have been under intensive study until today [9–17]. Much considerable effort has been devoted to enhancing the performance of new electrocatalysts for hydrazine electrooxidation for DHFCs [12,18–25]. Variety Ni-based binary catalysts were shown to improve hydrazine oxidation efficiently though alloying effects [26–33]. These improved performance levels motivated us to further study Ni-based binary and ternary catalysts for use in DHFCs.

The characteristic of combinatorial chemistry in the material R&D of drug discovery research has been known as a high-throughput screening and optimization of functional materials since the 1990s. In order to accelerate the catalyst development for the increasing demand on the fuel cell technology, combinatorial chemistry has been also attempted to adopt in the electrocatalyst development for fuel cells since 1998 [34–42]. Furthermore, various high throughput electrocatalyst screening methods have been reported including optical screening [34,43], scanning electrochemical microscopy [44], multi-electrode half-cell [45–47], and multi-electrode full cell [48]. In this study, carbon supported binary Ni–M (with M = Mn, Fe, Zn, La) and ternary Ni–Mn–Fe and Ni–Zn–La catalysts were synthesized using impregnation/freeze-drying procedure. All prepared 79 samples were evaluated in their catalytic activity using the temperature controlled (4 × 4) 16-channel electrochemical combinatorial array for hydrazine oxidation in alkaline media for rapid parallel screening.

2. Experimental

2.1. Temperature controlled 16-channel electrochemical combinatorial array and fabrication

Fig. 1 shows the modified 16-channel electrochemical combinatorial array that allows temperature control of the electrochemical cells using a water bath. The device is based on an array previously developed by K.C. Neyerlin et al. [45]. The equipment is used for the catalyst screening at a temperature close to the operating temperature of DHFCs. Fig. 1a shows a side view of four array chambers, machined out of polyvinylidene fluoride (PVDF), with their independent reference Zn/ZnO electrodes and Pt counter electrodes. Each of the 16 counter and reference electrodes were connected to a circuit board, which was then connected to the multi-channel potentiostat (1470E, Solartron Analytical). The top sections of the array, the PVDF chambers, and the circuit board are removable to enable easy catalyst dispensing onto and cleaning of the grassy carbon (GC) electrodes. The GC electrodes are polished with alumina paste. The bottom of each polyetheretherketone (PEEK) chamber was sealed with an O-ring to prevent any electrolyte and water leakage. Prior to the attachment of the circuit board onto the PVDF, a separate 16-tube parallel bubbler attachment was used to purge the array with nitrogen; the flow of gas was then switched to “blanketing” in a fashion similar to that of a traditional rotating disk electrode setup. Fig. 1b shows a top down view of a 4 × 4 array of GC disks each having an active area of 0.785 cm^2 (10 mm diameter) sealed in PEEK. Fig. 1c displays the side view of one of the cells. Gold pin connectors are used in order to provide electrical contact between the GC disks and the wire harness connection to the multi-channel potentiostat.

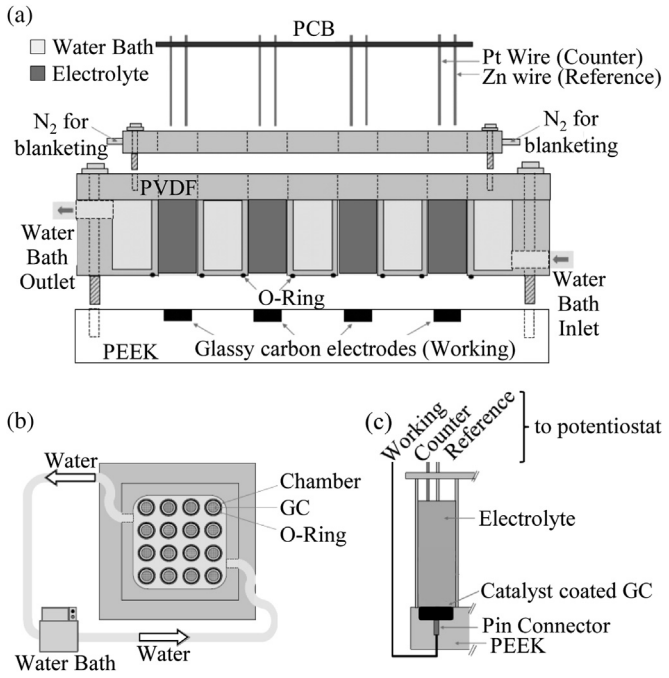

Fig. 1. Schematics of a variable temperature 16-channel combinatorial electrochemical screening array cell. (a) Cross-sectional view of the screening cell with individual chambers, electrolyte, reference electrode, counter electrode, and working electrode, (b) top view of GC working electrode array, (c) cross-sectional view of electrode showing the use of pin connector to connect the potentiostat to the bottom of GC electrode.

2.2. Catalyst synthesis

2.2.1. Impregnation/freeze-drying procedure for the catalyst screening

The carbon supported binary and ternary catalyst libraries were synthesized using an impregnation/freeze-drying procedure followed by thermal annealing for the screening test. The reference catalysts such as Ni/C, Mn/C, Fe/C, Zn/C, and La/C were prepared by the same method. All catalysts samples contained 23 wt% total metal on carbon support. First, aqueous metal nitrate solutions (Kishida Chemical) dissolved in deionized water (>18.2 MΩ cm, Millipore Direct-Q 3 UV Water Purification System, Millipore) were impregnated with carbon black (ECP600JD, Lion Corp.) by a robotic liquid dispenser (Model GX271, Gilson) utilized to pipette the desired amount of metal solution. Slurries were sonicated for 5 min and the impregnated catalysts were then immersed in liquid N_2. The cooled slurries were freeze-dried under a moderate vacuum (0.055 mbar, FreeZone, Labconco) over 40 h. All catalysts were prepared in 10 mL quartz vials. Reduction of metal precursors to the zero-valent state on the carbon support was thermally driven under a reductive H_2 atmosphere (10% H_2, balance Ar) at 250 °C for 2.5 h using a tube furnace. Final thermal annealing was performed immediately after the reduction step at 800 °C for 5 h in 10% H_2 in Ar. The catalysts including Zn such as Zn/C, Ni–Zn/C, and Ni–Zn–La/C were annealed at 400 °C for 5 h in the final reduction to prevent the sublimation of Zn.

2.2.2. Spray pyrolysis for MEA anode catalyst

Synthesis of unsupported $Ni_{0.87}Zn_{0.13}$ and $Ni_{0.9}La_{0.1}$ catalysts were achieved using spray pyrolysis following a previously reported approach [26,27]. Metal nitrates (Ni, Zn, and La) (Sigma–Aldrich Co.) were dissolved in 10% HNO_3 solution to a final concentration of 5% of specific stoichiometric ratios. The dissolved bimetallic solution was atomized (Model 3076, TSI Inc.) and

pyrolyzed through a furnace at 700 °C using N_2 as the carrier gas. Pyrolyzed particles were collected on a Teflon filter and air dried. Alloys were formed by reduction of the oxide powders under 5% H_2 in N_2 at 500 °C.

2.3. Evaluation of catalytic activity

2.3.1. Electrochemical measurement using a (4 × 4) 16-channel electrochemical electrode array

Catalyst inks were prepared in the following manner. A 10 mg of the desired catalyst was combined with 7.5 mL of DI water, 1.5 mL of isopropanol, 0.46 mL of THF and 0.04 mL of a 5 wt% anionic ionomer solution (A3, Tokuyama). The ink was then sonicated during 15 min. After sonication, a 0.04 mL of the ink was applied onto the GC electrode, resulting in a loading of 0.054 mg cm^{-2}. The entire array was then left to dry for at least 1 h.

A (4 × 4) 16-channel electrochemical combinatorial array for parallel testing of prepared electrocatalysts was utilized in this study. The array consisted of mirror polished glassy carbon working electrodes where the different catalyst materials were applied. Each of these electrodes was in contact with independent samples of the testing solution, and independently controlled by the multipotentiostat. Due to the use of strong alkaline media, a Zn/ZnO quasi reference electrode was utilized instead of the conventional Hg/HgO reference electrode. The reference electrode consisted in a Zn wire immersed in 1.0 M KOH solution. The Zn/ZnO electrode was calibrated using a reversible hydrogen electrode (RHE). A Pt wire served as counter electrode. All potentials presented and discussed here are reported against a RHE at pH 14. Experiments were performed at 60 °C.

2.3.2. Measurement of DHFCs

A 100 mg of the catalyst was combined with 0.96 mL of isopropanol, 0.24 mL of THF and 0.2 mL of a 5 wt% anionic ionomer solution (A3, Tokuyama). The ink was then sonicated 5 min. After sonication, ZrO_2 beads (Diameter = 2.0 mm, Nikkato) were added and the mixture was agitated for 15 min. The prepared ink was directly sprayed onto an anionic electrolyte membrane (A201, Tokuyama). Co-PPY-C (PPY: polypyrrole) cathode catalyst was formed into an electrode using a similar method to that for the anode. The membrane was then pressed for 5 min at room temperature to bind the catalyst layers to the membrane. The membrane was then immersed in 1.0 M KOH solution for 8 h in order to exchange the anions to OH^-.

The prepared MEA, with a round shaped working electrode area of 1 cm^2, was inserted in a single cell to measure the cell performance. The fuel (1.0 M KOH + 20% $N_2H_4 \cdot H_2O$) was supplied to the anode at a flow rate of 2 ml min^{-1}, and air gas humidified at 50 °C was supplied to the cathode at the flow rate of 500 ml min^{-1}. The applied shape of the flow-fields was serpentine for the anode and comb-shaped for the cathode. The cell temperature was controlled at 80 °C. The differential operating pressures on anode side was 10 kPa and cathode side was 60 kPa.

2.4. Characterization of catalysts

Field emission scanning electron microscope (FE-SEM, SU8020, Hitachi High-Technologies Corporation) and energy dispersive X-ray spectroscopy (EDX, X-Max 80, HORIBA Ltd.) with the voltage acceleration of 15 kV were performed to analyze catalyst morphology and composition without any deposition on the catalyst surface. The crystal structures of the prepared catalysts were examined using the θ–2θ X-ray diffraction (XRD, RINT 2000, Rigaku) with the Cu Kα source of operating at a potential of 40 kV and a current of 450 mA. 2θ diffraction angles ranged from 10° to 110° at 5° min^{-1}.

3. Results and discussion

3.1. Evaluation of catalytic activity of binary libraries for hydrazine oxidation

The linear sweep voltammetry (LSV) profiles of binary catalyst libraries are shown in Fig. 2. A 16-channel electrochemical combinatorial array was used to evaluate the catalytic activity for hydrazine oxidation from −0.129 V to 0.221 V vs. RHE in 1 M KOH + 1 M hydrazine hydrate electrolyte at 60 °C. The onset potential is defined as the potential at 10.9 A g^{-1}, and mass activity is defined as the current per unit total metal weight at 0.221 V vs. RHE. The anodic peaks in the potential range from 0 V to 0.221 V vs. RHE are ascribed to hydrazine oxidation as shown in Fig. 2. The inset figure in each figure also clearly shows onset potentials of each catalyst for hydrazine oxidation. The LSV profiles of Ni–La/C catalyst library were

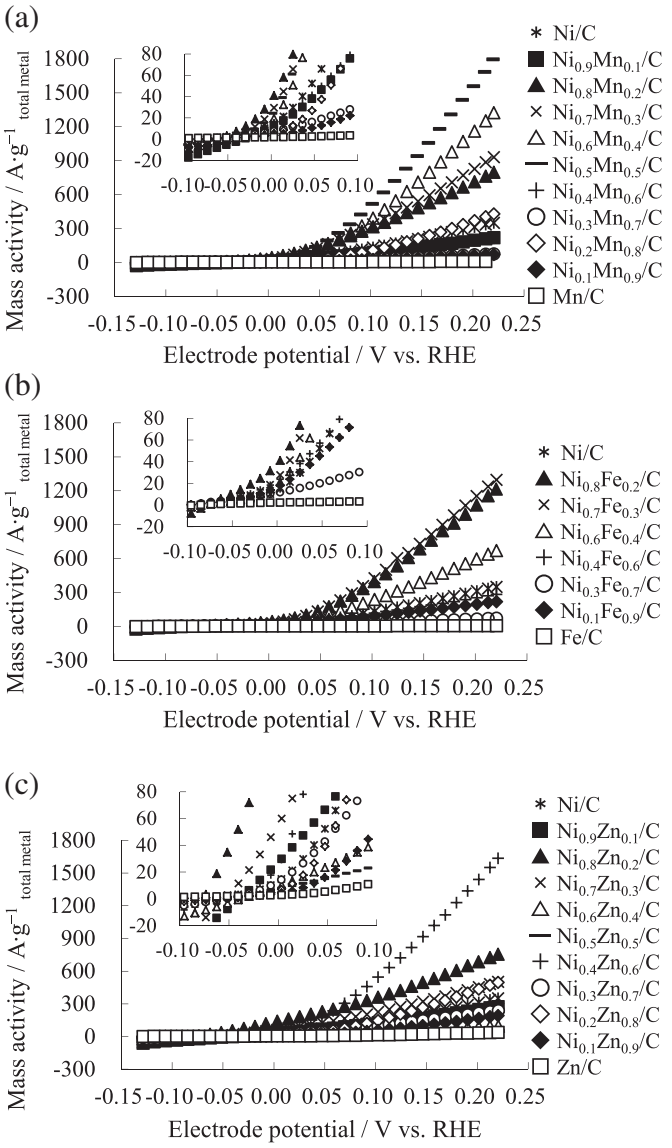

Fig. 2. LSV profiles of carbon supported binary catalysts at scanning rate of 20 mV s^{-1}. (a) Ni–Mn/C catalyst library, (b) Ni–Fe/C, (c) Ni–Zn/C. The LSV profiles of Ni–La/C catalyst library were described in the previous report of Ref. [33].

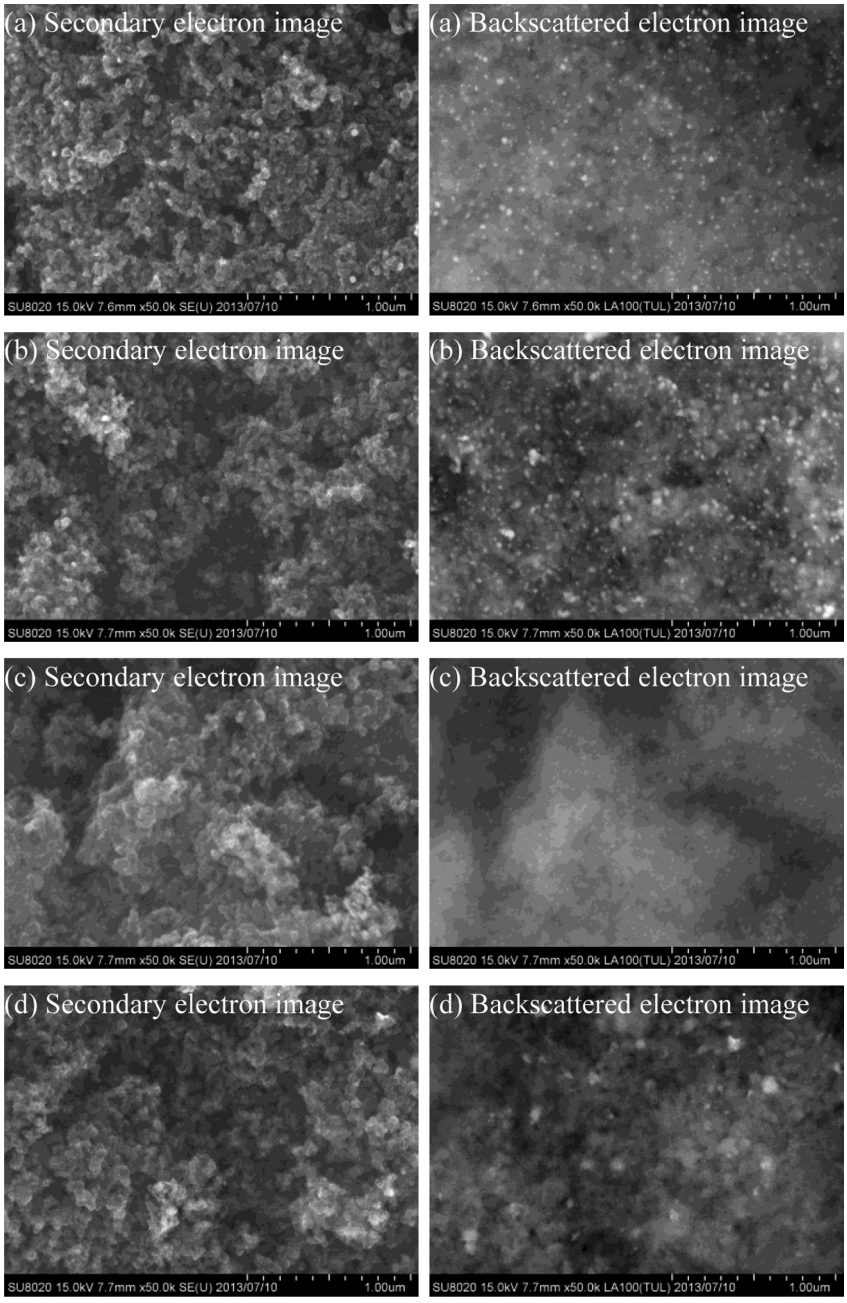

Fig. 3. SEM images of prepared catalysts. (a) Ni/C, (b) $Ni_{0.5}Mn_{0.5}$/C, (c) $Ni_{0.7}Fe_{0.3}$/C, (d) $Ni_{0.4}Zn_{0.6}$/C.

described in a previous report [33]. Fe/C, Mn/C, Zn/C, and La/C have no catalytic activity for hydrazine oxidation in this potential range. However the catalytic activity of Ni/C for hydrazine oxidation is improved by the addition of these elements as shown in Fig. 2. The mass activity of $Ni_{0.5}Mn_{0.5}$/C, $Ni_{0.7}Fe_{0.3}$/C, $Ni_{0.4}Zn_{0.6}$/C, and $Ni_{0.9}La_{0.1}$/C was higher in each binary library. H. Yang et al. reported on the activity of Ni–Fe catalysts with stoichiometries from $Ni_{0.55}Fe_{0.45}$ to $Ni_{0.95}Fe_{0.05}$ supported on multi wall carbon nanotubes (Ni–Fe/MWCNTs) synthesized by pulse reversal plating compared to the pure Ni/MWCNTs and Fe/MWCNTs in Ar-saturated 0.1 M hydrazine hydrate–0.015 M KOH–1 M NaCl solution [32]. This study finds $Ni_{0.85}Fe_{0.15}$/MWCNTs as the most active catalyst with a maximum mass activity of 1650 A g^{-1} at −0.45 V (vs. RHE) and an onset potential of −0.8 V. The catalysts with stoichiometries from $Ni_{0.70}Fe_{0.30}$/MWCNTs to $Ni_{0.95}Fe_{0.05}$/MWCNTs improve the catalytic activity for hydrazine oxidation against pure Ni/MWCNTs. Similar active permutation of mass activity is observed for the catalysts from $Ni_{0.6}Fe_{0.4}$/C to $Ni_{0.8}Fe_{0.2}$/C prepared by impregnation/freeze-drying procedure as shown in Fig. 2b. The onset potentials of the described above active binary catalysts are also shifted toward lower potential than Ni/C. Especially, the onset potential of $Ni_{0.8}Zn_{0.2}$/C and $Ni_{0.9}La_{0.1}$/C are drastically shifted when compared with Ni/C as shown in each inset figure. U. Martinez et al. reported on the activity and mechanism of unsupported Ni–Zn catalysts synthesized by spray pyrolysis [27]. $Ni_{0.87}Zn_{0.13}$ shows a better activity near the onset potential than $Ni_{0.33}Zn_{0.67}$, $Ni_{0.50}Zn_{0.50}$, and pure Ni. Similar performance is observed for $Ni_{0.8}Zn_{0.2}$/C catalyst as shown in Fig. 2c. The onset potential is more representative of catalyst intrinsic performance, because the overpotential of catalysts depends on electrochemical reaction potential between catalysts and hydrazine.

3.2. FE-SEM analysis

Fig. 3 shows SEM micrographs of Ni/C, $Ni_{0.5}Mn_{0.5}$/C, $Ni_{0.7}Fe_{0.3}$/C, and $Ni_{0.4}Zn_{0.6}$/C to analyze the relationship between metal particle sizes and mass activities. These binary catalysts have the highest mass activity in each binary library as shown in Fig. 2. The secondary electron (SE) images show the catalyst morphology and backscattered electron (BSE) images are used to detect contrast between areas with different chemical compositions. The similar morphology of prepared catalysts was observed in SE images of Fig. 3. The contrast in BSE images of Fig. 3 indicates the metal particle on the carbon support of prepared catalysts. Highly dispersive metal particles on the carbon support are observed as shown in BSE images of Fig. 3. The diameters of metal particles in Ni/C and $Ni_{0.5}Mn_{0.5}$/C were approximately estimated from 20 to 30 nm in BSE images of Fig. 3a and b. The diameter of metal particles in $Ni_{0.9}La_{0.1}$/C was confirmed to be similar to the metal particles in Ni/C as shown in a previous research [33]. The agglomerated metal particles from 50 to 100 nm were observed in $Ni_{0.4}Zn_{0.6}$/C as shown in Fig. 3d. The mass activities of $Ni_{0.5}Mn_{0.5}$/C, $Ni_{0.9}La_{0.1}$/C, and $Ni_{0.4}Zn_{0.6}$/C were increased through the intrinsic electrochemical activity. Meanwhile the $Ni_{0.7}Fe_{0.3}$/C has smaller metal particles than metal particles in Ni/C, and they were examined 10 nm from BSE image in Fig. 3c. The high mass activity of $Ni_{0.7}Fe_{0.3}$/C for hydrazine oxidation is supported to be due to both intrinsic electrochemical activity and surface area.

Table 1 shows the atomic ratio of $Ni_{0.5}Mn_{0.5}$/C, $Ni_{0.7}Fe_{0.3}$/C, and $Ni_{0.4}Zn_{0.6}$/C to investigate the chemical composition of each binary catalyst in the entire view range of three different areas at ×50.0 k by EDX. The average composition well agrees with the starting values used for the preparation. The binary catalysts were prepared with well-controlled alloy composition using an impregnation/freeze-drying procedure followed by thermal annealing.

3.3. Optimization of catalysts for hydrazine oxidation using combinatorial chemistry

The activity-composition map of onset potential for hydrazine oxidation of Ni–Mn–Fe/C and Ni–Zn–La/C including binary catalyst library and reference catalysts are shown in Fig. 4. The catalyst activity was represented with circles showing tones from white to black. Ni/C catalyst as a reference material was shown in white color, and the catalysts which have lower catalytic activity (higher the onset potential) than Ni/C were also shown in white color. The high active materials in the ternary catalyst libraries for hydrazine oxidation are confirmed in the proximity of active composition of the binary catalyst library as shown by the dotted circles of Fig. 4. $Ni_{0.6}Mn_{0.2}Fe_{0.2}$/C and $Ni_{0.8}Zn_{0.1}La_{0.1}$/C catalysts showed the highest hydrazine electrooxidation activity at each composition region as shown in Fig. 4a and b, respectively. These catalysts constitute a promising new candidate with enhanced activity at DHFC anodes. Such activity maps conveniently facilitate the selection of a suitable catalyst candidate for hydrazine oxidation. Compared to a Ni/C catalyst, the optimized ternary catalysts, $Ni_{0.6}Mn_{0.2}Fe_{0.2}$/C and $Ni_{0.8}Zn_{0.1}La_{0.1}$/C, were able to oxidize the hydrazine in alkaline media at lower potential. In Ni-based binary system, addition of Zn and La for ranges from 10 to 20 at% in Ni is effective for hydrazine oxidation. Moreover, the addition of Fe–Mn and Zn–La for ranges from 20 to 40 at% is significantly effective for the improvement of the electrocatalytic activity for hydrazine oxidation.

Table 1
Atomic ratio of $Ni_{0.5}Mn_{0.5}$/C, $Ni_{0.7}Fe_{0.3}$/C, and $Ni_{0.4}Zn_{0.6}$/C.

Catalyst	Average atomic ratio (%)				Standard deviation			
	Ni K	Mn K	Fe K	Zn K	Ni K	Mn K	Fe K	Zn K
$Ni_{0.5}Mn_{0.5}$/C	54.8	45.2			0.1	0.1		
$Ni_{0.7}Fe_{0.3}$/C	72.8		27.2		0.6		0.6	
$Ni_{0.4}Zn_{0.6}$/C	38.2			51.8	0.8			0.8

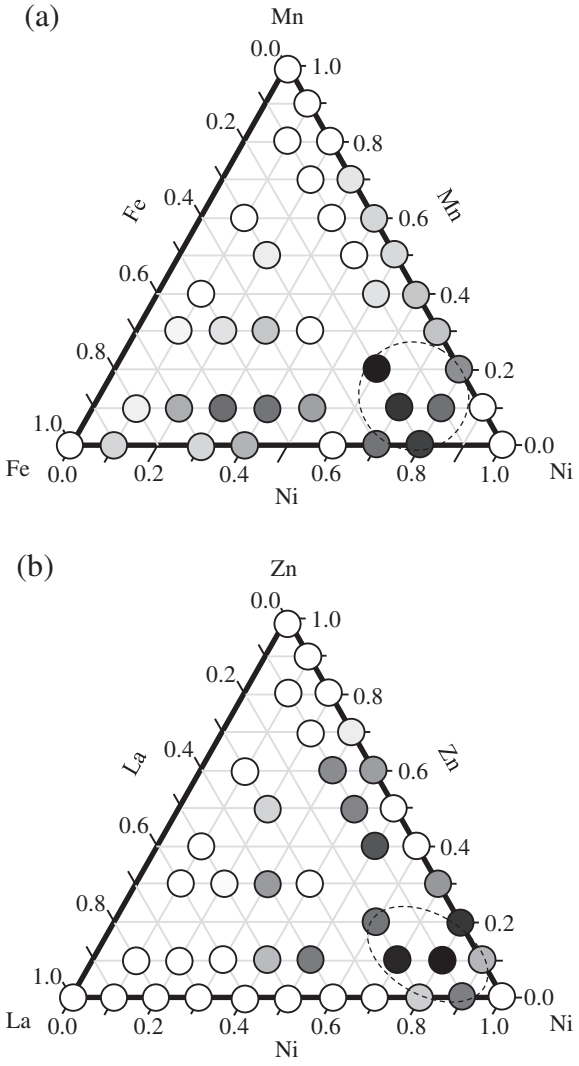

Fig. 4. Activity-composition map of onset potential of carbon supported ternary catalyst library (1 M KOH + 1 M hydrazine hydrate). (a) Ni–Mn–Fe/C, (b) Ni–La–Zn/C. Both maps encode activity by color from black to white. Ni/C catalyst as a reference was exhibited white color, and catalysts that have lower activity than Ni/C were also shown white color.

3.4. MEA performances

From the results of the optimization of ternary catalysts by combinatorial chemistry, $Ni_{0.6}Fe_{0.2}Mn_{0.2}$/C and $Ni_{0.8}Zn_{0.1}La_{0.1}$/C catalysts were used as an anode catalyst for DHFCs, together with Ni/C reference catalyst for comparison as shown in Fig. 5a. Co-PPY-C (PPY: polypyrrole) was used as a cathode catalyst. Error bars in Fig. 5 exhibit the standard deviation to discuss the significant difference of prepared catalysts against reference Ni catalyst. Power density of the cell using $Ni_{0.8}Zn_{0.1}La_{0.1}$/C and $Ni_{0.6}Fe_{0.2}Mn_{0.2}$/C catalysts reached to 211 mW cm^{-2} and 224 mW cm^{-2} respectively that were higher than that of the cell using Ni/C reference catalyst as shown in Fig. 5a. The open circuit voltage (OCV) of 0.734 V and 0.715 V were achieved when cell was operated at 80 °C using $Ni_{0.8}Zn_{0.1}La_{0.1}$/C and $Ni_{0.6}Fe_{0.2}Mn_{0.2}$/C catalysts respectively.

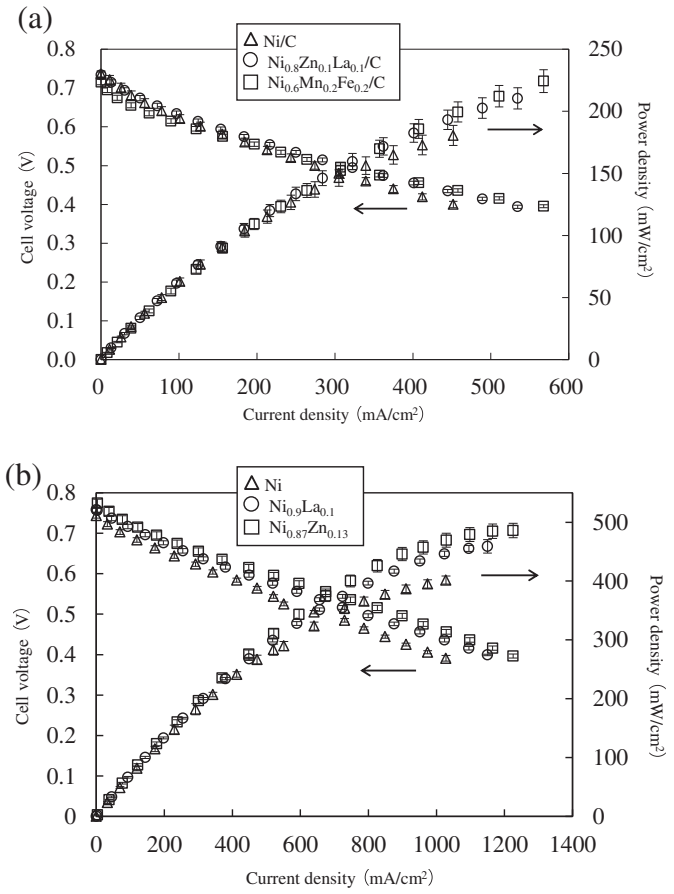

Fig. 5. Cell performances of DHFC. (a) Ni/C, $Ni_{0.8}Zn_{0.1}La_{0.1}/C$, and $Ni_{0.6}Mn_{0.2}Fe_{0.2}/C$ catalysts as an anode, (b) unsupported Ni, $Ni_{0.9}La_{0.1}$ and $Ni_{0.87}Zn_{0.13}$ catalysts as an anode.

Optimized ternary catalysts by combinatorial chemistry contributed to improve the cell performance of DHFCs.

From the results of binary catalyst studied in our previous research [27] and binary catalyst survey using combinatorial chemistry, unsupported $Ni_{0.87}Zn_{0.13}$ and $Ni_{0.9}La_{0.1}$ catalysts which were synthesized by spray pyrolysis were considered as an anode catalyst for DHFCs. Fig. 5b shows the cell performances of DHFCs using unsupported $Ni_{0.87}Zn_{0.13}$ and $Ni_{0.9}La_{0.1}$ as an anode catalyst, together with conventional Ni catalyst (210H, INCO) as a reference catalyst. The cell performance of DHFCs was increased by using unsupported Ni catalyst compared with Ni/C. These results suggest that the design of anode catalyst layer affects the cell performance of DHFCs. There is the significant difference of cell performances of DHFCs between unsupported binary catalysts and pure Ni catalyst as shown in error bars of each catalyst in Fig. 5b. The DHFCs showed high performance without precious metal catalysts on either anode or cathode, as shown in Fig. 4. When Ni, $Ni_{0.87}Zn_{0.13}$, and $Ni_{0.9}La_{0.1}$ were used as an anode catalyst in DHFCs, their OCV were observed as 0.744 V, 0.777 V, and 0.758 V, respectively. The difference in observed OCV between $Ni_{0.87}Zn_{0.13}$, $Ni_{0.9}La_{0.1}$, and Ni relate to the improved onset potential for hydrazine oxidation when Zn (or La) is added to Ni. The maximum power density for $Ni_{0.87}Zn_{0.13}$ and $Ni_{0.9}La_{0.1}$ are 486 mW cm^{-2} and 459 mW cm^{-2} respectively, which are 21% and 14% higher than the 401 mW cm^{-2} obtained for the pure Ni catalyst. The improved performance of the unsupported $Ni_{0.87}Zn_{0.13}$ and $Ni_{0.9}La_{0.1}$ catalysts when compared to the Ni confirms the results of the carbon supported $Ni_{1-x}Zn_x$ and $Ni_{1-x}La_x$ ($0.1 \leq x \leq 0.9$) catalysts where the $Ni_{0.8}Zn_{0.2}/C$ and $Ni_{0.9}La_{0.1}/C$

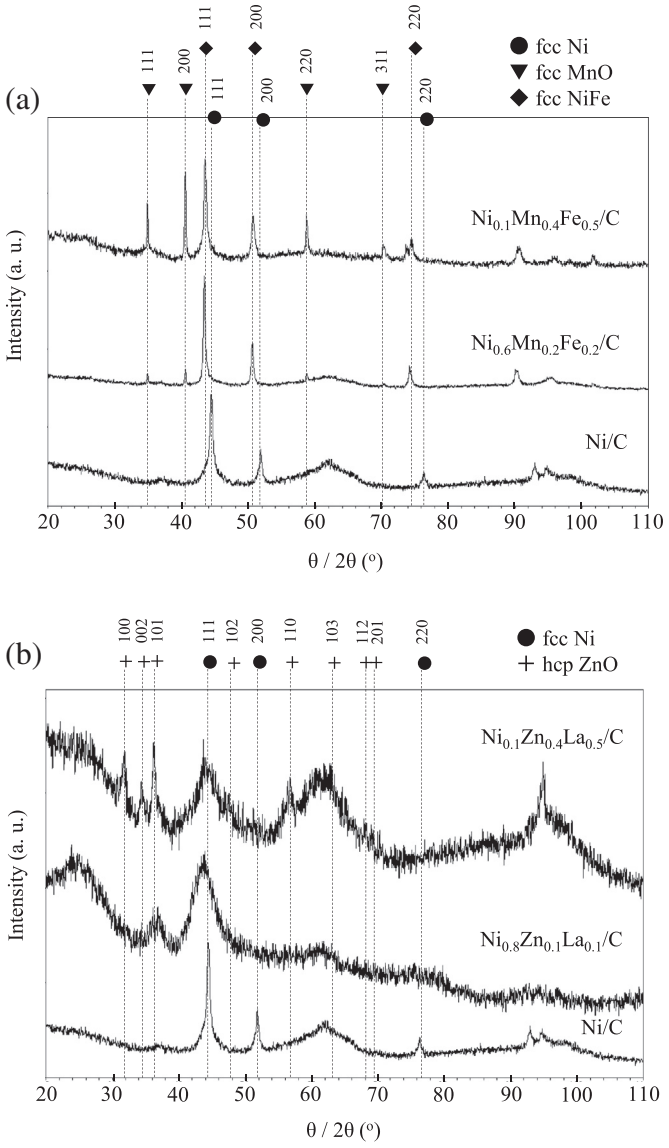

Fig. 6. XRD spectra of ternary library to compare between active catalysts and inactive catalysts together with Ni/C as a reference catalyst. (a) Ni–Mn–Fe/C, (b) Ni–Zn–La/C.

formulations were the best performing anode catalysts in the Ni-based binary system for DHFCs.

3.5. XRD analysis

XRD analysis was performed to obtain and compare insights on the crystal structure between the ternary most active catalysts ($Ni_{0.6}Mn_{0.2}Fe_{0.2}/C$ and $Ni_{0.8}Zn_{0.1}La_{0.1}/C$) and the lowest activity catalysts ($Ni_{0.1}Mn_{0.4}Fe_{0.5}/C$ and $Ni_{0.1}Zn_{0.4}La_{0.5}/C$) for hydrazine oxidation together with a reference Ni/C catalyst as shown in Fig. 6. Fig. 6a shows the XRD spectra of the Ni–Mn–Fe/C catalysts to compare Ni/C. Almost all diffraction peaks of the reference Ni/C catalyst were attributed to the fcc Ni with PDF-04-0850. The broad peak near the 60° observed in Ni/C is attributed to Ni-oxide or the carbon support. The diffraction peaks from fcc MnO with PDF-07-0230 were clearly observed in $Ni_{0.1}Mn_{0.4}Fe_{0.5}/C$. In the $Ni_{0.6}Mn_{0.2}Fe_{0.2}/C$ catalyst, X-ray intensity from MnO was lower than that in $Ni_{0.1}Mn_{0.4}Fe_{0.5}/C$. The diffraction peaks of $Ni_{0.1}Mn_{0.4}Fe_{0.5}/C$ at 2θ values of 43.6°, 50.8°, and 74.7° can be assigned to the (111),

(200), and (220) crystal planes of the fcc Ni–Fe alloy with PDF-47-1405. Meanwhile, the diffraction peaks except for MnO in $Ni_{0.6}Mn_{0.2}Fe_{0.2}$/C slightly downward shifted from 2θ values fcc Ni–Fe alloy in $Ni_{0.1}Mn_{0.4}Fe_{0.5}$/C is due to the incorporation of Mn. This peak shift in $Ni_{0.6}Mn_{0.2}Fe_{0.2}$/C due to the random substitution of Ni or Fe atoms with Mn atoms while retaining the fcc Ni–Fe crystal structure. Although the crystal structure is maintained, lattice spacing changes due to the difference in atomic size causes a shift in the XRD spectrum.

Fig. 6b shows the XRD spectra of Ni–Zn–La/C and Ni/C catalysts for comparison. The diffraction peaks from hcp ZnO with PDF-36-1451 were confirmed in $Ni_{0.1}Zn_{0.4}La_{0.5}$/C. However, the diffraction peaks for La-oxide were not observed in both $Ni_{0.1}Zn_{0.4}La_{0.5}$/C and $Ni_{0.8}Zn_{0.1}La_{0.1}$/C catalysts, either because the La is amorphous or the oxide particles, which have low X-ray cross sections, are too small to be detected by XRD [33]. The broad diffraction peaks from 40° to 48° were observed in both $Ni_{0.1}Zn_{0.4}La_{0.5}$/C and $Ni_{0.8}Zn_{0.1}La_{0.1}$/C catalysts due to a component of amorphous fcc Ni structure with lower annealing temperature at 400 °C to prevent the sublimation of Zn from samples. The maximum of these broad peaks is shifted toward lower 2θ values more than the 44.5° in Ni/C case. Therefore another possible cause of peak broadening might be the existence of two-phase crystal structures for the fcc Ni and Ni–Zn–La alloy. Ni–Zn–La alloy in $Ni_{0.8}Zn_{0.1}La_{0.1}$/C were supposed to form the alloy retaining a fcc Ni structure due to the Ni rich composition.

The active catalysts for hydrazine oxidation showed predominantly the fcc Ni-based alloy structure type according to the XRD results, with optimal activity for compositions near $Ni_{0.6}Mn_{0.2}Fe_{0.2}$ and $Ni_{0.8}Zn_{0.1}La_{0.1}$. The reason for a better catalytic activity for hydrazine oxidation of $Ni_{0.6}Mn_{0.2}Fe_{0.2}$/C and $Ni_{0.8}Zn_{0.1}La_{0.1}$/C is related with the Ni alloying with added elements such as Fe, Mn, Zn, and La. These metals intrinsically modify the catalytic activity of Ni by an alloying effect.

4. Conclusions

Ni-based binary and ternary systems have been explored for the electrocatalytic hydrazine oxidation by using combinatorial chemistry. Ni-based anode catalyst for hydrazine electrooxidation showed improved catalytic activity by addition of Zn, La, Mn, and Fe. $Ni_{0.8}Zn_{0.2}$/C and $Ni_{0.9}La_{0.1}$/C were able to oxidize the hydrazine at lowest potential in the binary library. In ternary libraries, $Ni_{0.6}Mn_{0.2}Fe_{0.2}$/C and $Ni_{0.8}Zn_{0.1}La_{0.1}$/C also exhibited effective catalytic activity for hydrazine oxidation. Unsupported binary $Ni_{0.87}Zn_{0.13}$ and $Ni_{0.9}La_{0.1}$ catalysts showed 486 mW cm^{-2} and 459 mW cm^{-2} respectively for MEA performances in a DHFC. XRD analysis showed that fcc Ni-based alloy structure type increases the catalytic activity of Ni by an alloying effect. Combinatorial chemistry was a useful procedure to accelerate and optimize the electrocatalyst discovery for DHFCs.

Acknowledgments

We would like to thank Professor Dr. N. Mizuno and Associate Professor Dr. K. Yamaguchi (Tokyo Univ.) for their advice on catalyst research. The authors thank Hokko Chemical Industry Co., Ltd. for synthesis of Co-PPY-C.

References

[1] S. Karp, L. Meites, J. Am. Chem. Soc. 84 (1962) 906.
[2] A. Kunugi, Z. Takehara, S. Yoshizawa, Denkikagaku 33 (1965) 211.
[3] G.E. Evans, K.V. Kordesch, Science 158 (1967) 1148.
[4] S. Takahashi, S. Higuchi, R. Fujii, Y. Miyake, Report of Governmental Industrial Research Institute, vol. 346, Osaka, 1974.
[5] K. Yamada, K. Yasuda, N. Fujiwara, Z. Siroma, H. Tanaka, Y. Miyazaki, T. Kobayashi, Electrochem. Commun. 5 (2003) 892.
[6] K. Asazawa, K. Yamada, A. Oka, M. Taniguchi, T. Kobayashi, Angew. Chem., Int. Ed. 46 (2007) 8024.
[7] W.X. Yin, Z.P. Li, J.K. Zhu, H.Y. Qin, J. Power Sources 182 (2008) 520.
[8] A. Serov, C. Kwak, Appl. Catal. B: Environ. 98 (2010) 1.
[9] B.E. Conway, N. Marincic, D. Gilroy, E. Rudd, J. Electrochem. Soc. 113 (1966) 1144.
[10] R. Furumi, T. Iwaki, M. Fukuda, Denkikagaku 36 (1968) 448.
[11] K. Korinek, J. Koryta, M. Musilova, J. Electroanal. Chem. 21 (1969) 319.
[12] K. Tamura, T. Kahara, J. Electrochem. Soc. 123 (1976) 776.
[13] G. Ramis, M.A. Larrubia, Mol. Catal. A Chem. 215 (2004) 161.
[14] K. Asazawa, K. Yamada, H. Tanaka, M. Taniguchi, K. Oguro, J. Power Sources 191 (2009) 362.
[15] K. Asazawa, T. Sakamoto, S. Yamaguchi, H. Fujikawa, H. Tanaka, K. Oguro, J. Electrochem. Soc. 156 (2009) B509.
[16] M.K. Agusta, M. David, H. Nakanishi, H. Kasai, Surf. Sci. 604 (2010) 245.
[17] M.K. Agusta, H. Kasai, Surf. Sci. 606 (2012) 766.
[18] Y. Fukumoto, T. Matsunaga, T. Hayashi, Electrochim. Acta 26 (1981) 633.
[19] K. Yamada, K. Asazawa, K. Yasuda, T. Ioroi, H. Tanaka, Y. Miyazaki, T. Kobayashi, J. Power Sources 115 (2003) 236.
[20] K. Yamada, K. Yasuda, H. Tanaka, Y. Miyazaki, T. Kobayashi, J. Power Sources 122 (2003) 132.
[21] G. Gao, D. Guo, C. Wang, H. Li, Electrochem. Commun. 9 (2007) 1582.
[22] E. Granot, B. Filanov, I. Presman, I. Kuras, F. Patolsky, J. Power Sources 204 (2012) 116.
[23] C.-C. Yang, A.S. Kumar, M.-C. Kuo, S.-H. Chien, J.-M. Zen, Anal. Chim. Acta 554 (2005) 66.
[24] J.S. Pinter, K.L. Brown, P.A. DeYoung, G.F. Peaslee, Talanta 71 (2007) 1219.
[25] S. Yamazaki, T. Ioroi, K. Tanimoto, K. Yasuda, K. Asazawa, S. Yamaguchi, H. Tanaka, J. Power Sources 204 (2012) 79.
[26] U. Martinez, K. Asazawa, B. Halevi, T. Olson, B. Kiefer, A.K. Datye, H. Tanaka, P. Atanassov, ECS Trans. 33 (2010) 1673.
[27] U. Martinez, K. Asazawa, B. Halevi, A. Falase, B. Kiefer, A. Serov, M. Padilla, T. Olson, A. Datye, H. Tanaka, P. Atanassov, Phys. Chem. Chem. Phys. 14 (2012) 5512.
[28] J. Sanabria-Chinchilla, K. Asazawa, T. Sakamoto, K. Yamada, H. Tanaka, P. Strasser, J. Am. Chem. Soc. 133 (2011) 5425.
[29] T. Sakamoto, K. Asazawa, K. Yamada, H. Tanaka, Catal. Today 164 (2011) 181.
[30] L.Q. Ye, Z.P. Li, H.Y. Qin, J.K. Zhu, B.H. Liu, J. Power Sources 196 (2011) 956.
[31] Y. Qingfeng, L. Lei, Y. Wenqiamg, L. Xiaoping, Z. Zhihua, N. Huidong, Rare Met. 29 (2010) 26.
[32] H. Yang, X. Zhong, Z. Dong, J. Wang, J. Jin, J. Ma, RSC Adv. 2 (2012) 5038.
[33] T. Sakamoto, K. Asazawa, U. Martinez, B. Halevi, T. Suzuki, S. Arai, D. Matsumura, Y. Nishihata, P. Atanassov, H. Tanaka, J. Power Sources 234 (2013) 252.
[34] E. Reddington, A. Sapienza, B. Gurau, R. Vishwanathan, S. Sarangapani, E.S. Smotkin, T.E. Mallouk, Science 280 (1998) 1735.
[35] P. Strasser, Q. Fan, M. Devenney, W.H. Weinberg, P. Liu, J.K. Norskov, J. Phys. Chem. B 107 (2003) 11013.
[36] J.F. Whitacre, T. Valdez, S.R. Narayanan, J. Electrochem. Soc. 152 (2005) A1780.
[37] S. Jayaraman, S.-H. Baeck, T.F. Jaramillo, A. Kleiman-Shwarsctein, E.W. McFarland, Rev. Sci. Instrum. 76 (2005) 062227.
[38] P. Strasser, J. Comb. Chem. 10 (2008) 216.
[39] Y. Zhang, P.J. McGinn, J. Power Sources 206 (2012) 29.
[40] I. Cerri, T. Nagami, J. Davies, C. Mormiche, A. Vecoven, B. Hayden, Int. J. Hydrogen Energy 38 (2013) 640.
[41] R. Forgie, G. Bugosh, K.C. Neyerlin, Z. Liu, P. Strasser, Electrochem. Solid State Lett. 13 (2010) B36.
[42] A. Hagemeyer, P. Strasser, A.F. Volpe (Eds.), High-throughput Screening in Chemical Catalysis Technologies, Strategies and Applications, Wiley VCH, Weinheim, Germany, 2004.
[43] Y. Yamada, A. Ueda, H. Shioyama, T. Kobayashi, Appl. Surf. Sci. 223 (2004) 102.
[44] M. Black, J. Cooper, P. McGinn, Chem. Eng. Sci. 59 (2004) 4839.
[45] K.C. Neyerlin, G. Bugosh, R. Forgie, Z. Liu, P. Strasser, J. Electrochem. Soc. 156 (2009) B363.
[46] A.D. Spong, G. Vitins, S. Guerin, B.E. Hayden, A.E. Russell, J.R. Owen, J. Power Sources 119 (2003) 778.
[47] B.E. Hayden, D. Pletcher, J.P. Suchsland, L.J. Williams, Phys. Chem. Chem. Phys. 11 (2009) 1564.
[48] R. Jiang, D. Chu, J. Electroanal. Chem. 527 (2002) 137.